Flat-band spin dynamics and phonon anomalies of the saw-tooth spin-chain system $Fe_2O(SeO_3)_2$

V. P. Gnezdilov,[1,2] Yu. G. Pashkevich,[3] V. S. Kurnosov,[1] O. V. Zhuravlev,[3] D. Wulferding,[2,4] P. Lemmens,[2,4] D. Menzel,[2]
E. S. Kozlyakova,[5] A. Yu. Akhrorov,[5] E. S. Kuznetsova,[5] P. S. Berdonosov,[5] V. A. Dolgikh,[5]
O. S. Volkova,[5,6,7] and A. N. Vasiliev[5,6,7]

[1]*B.I. Verkin Institute for Low Temperature Physics and Engineering, NASU, 61103 Kharkiv, Ukraine*
[2]*Institute for Condensed Matter Physics, TU Braunschweig, D-38106 Braunschweig, Germany*
[3]*O.O. Galkin Donetsk Institute for Physics and Engineering, NASU, 03680 Kyiv-Kharkiv, Ukraine*
[4]*Laboratory for Emerging Nanometrology (LENA), TU Braunschweig, D-38106 Braunschweig, Germany*
[5]*Physics Faculty, M.V. Lomonosov Moscow State University, 119991 Moscow, Russia*
[6]*National University of Science and Technology MISiS, 119049 Moscow, Russia*
[7]*National Research South Ural State University, 454080 Chelyabinsk, Russia*

Fe^{3+} $S = 5/2$ ions form saw-tooth-like chains along the a axis of the oxoselenite $Fe_2O(SeO_3)_2$ and an onset of long-range magnetic order is observed for temperatures below $T_C = 105$ K. This order leads to distinct fingerprints in phonon mode linewidths and energies as resolved by Raman scattering. In addition, new excitations with small linewidths emerge below $T = 150$ K, and are assigned to two-magnon scattering processes with the participation of flat-band and high energy magnon branches. From this a set of exchange coupling constants is estimated. The specific ratio of the saw-tooth spine-spine and spine-vertex interactions may explain the instability of the dimer quantum ground state against an incommensurate 3D magnetic order.

I. INTRODUCTION

There is great interest in magnetic quantum systems with well known magnetic ground states and complex excitation spectra. One such system is the antiferromagnetic saw-tooth chain, or Δ chain—a one-dimensional lattice spin system with a topology of corner-sharing antiferromagnetically connected triangles. In contrast to many other frustrated systems, the ground state of a perfect $S = 1/2$ saw-tooth chain with couplings between the base (J_{bb}) and the base-vertex neighbor-nearest (NN) spins (J_{bv}) is exactly known [1–3]. It consists of a twofold degenerate superposition of spin singlets on either each left pair or each right pair of spins. Such a $J_{bb} = J_{bv} = J$ saw-tooth chain has a dispersionless small gap $\Delta = 0.215J$ [2–4] with the lowest excitations created by "kink" and "antikink" pairs. These are topological defects with spin $S = 1/2$. Further studies revealed a variety of ground states considering various ratios of J_{bb}/J_{bv} [4], Ising and Heisenberg bonds and spin-lattice interaction [5,6], Dzyaloshinskii-Moriya interactions (DMI) [7], or different spin states on the corners of triangles [8].

The saw-tooth lattice topology implies the presence of magnetic ions in at least two different Wyckoff positions. Thus, an interplay between different magnetic order parameters and geometrical frustration may yield a rich magnetic phase diagram. An easy switching between different three-dimensional (3D) ordered ground states requires a complex and unusual spin dynamics with the presence of a few low energy magnon modes. The latter modes might originate from zero energy flat-band modes activated by exchange interactions which are slightly different from characteristic interactions of the ideal saw-tooth structure. In the classical

limit some saw-tooth model systems possess zero energy flat-band modes, remarkably similar to a Kagome antiferromagnet [9,10]. Strongly correlated flat-band systems with localized magnon states in high magnetic fields are the subject of intensive studies (for a review see also Ref. [11]), as flat-band modes offer promising possibilities for manipulating the propagation of waves of any origin [12–14]. Therefore, they are of great interest for the development of magnonic devices [15]. For a device based on a saw-tooth photonic lattice a dedicated inhibition of transport has recently been reported together with a highly degenerate flat band [16]. A high energy magnon flat-band mode has been observed in a Kagome lattice ferromagnet in the absence of magnetic fields [17].

Despite this theoretical effort, only a small number of respective experimental realizations exists. This includes the delafossite $YCuO_{2.5}$ [18,19], olivines ZnL_2S_4 ($L = $ Er, Tm, Yb) [20], Mn_2GeO_4 [21–23], euchroite $Cu_2(AsO_4)(OH) \cdot 3H_2O$ [24], $CuFe_2Ge_2$ [25], oxy-arsenate $Rb_2Fe_2O(AsO_4)_2$ [26], and the nanotorus $[Fe_{10}Gd_{10}(Me\text{-}tea)_{10}(Me\text{-}teaH)_{10}(NO_3)_{10}] \cdot 20MeCN$ [27]. These compounds have been found to be of saw-tooth chain type realizing different cases of complex magnetism. Experimentally, no long-range magnetic order has been found in $YCuO_{2.5}$, ZnL_2S_4, and $Cu_2(AsO_4)(OH) \cdot 3H_2O$ even at low temperatures. In $Cu_2(AsO_4)(OH) \cdot 3H_2O$ a large spin gap of about $\Delta_0 = 90 \pm 5$ K and a new midgap of about $\Delta_M = 56$ K have been found in NMR and high field magnetization data, respectively.

With respect to 3D ordered ground states the most prominent representative is Mn_2GeO_4 with $T_{N1} = 47$ K and additional first-order magnetic transitions at $T_{N2} = 17$ K and

$T_{N3} = 5.5$ K [21–23]. Here the double-Q magnetic structure in the multiferroic state can be regarded as a canted conical spiral spin state. The saw-tooth compound $Rb_2Fe_2O(AsO_4)_2$ orders antiferromagnetically (AFM) below $T_N = 25$ K. Here an external magnetic field leads to a transition from an AFM to a ferrimagnetic state. Neutron diffraction on $CuFe_2Ge_2$ revealed AFM order below ≈ 175 K and an incommensurate spin structure (IC) below ≈ 125 K [25].

Here we report a Raman scattering study accompanied by magnetic susceptibility measurements of a new saw-tooth chain compound—the iron oxoselenite $Fe_2O(SeO_3)_2$. Unlike other saw-tooth chain compounds, its magnetic susceptibility evidences low-dimensional behavior above $T_C \sim 105$ K which cannot be described by a Curie-Weiss law. This highlights the proximity of $Fe_2O(SeO_3)_2$ to a quantum critical point (QCP). Below T_C the susceptibility follows antiferromagnetic behavior. We observe several phonon anomalies related to the onset of 3D magnetic order in $Fe_2O(SeO_3)_2$. Our lattice dynamic calculations support magnetoelastic coupling between lattice and magnetic subsystems. Below T_C we observe a few highly polarized and relatively narrow magnetic excitations at different energy scales. We assign these signals to two-magnon scattering with the participation of weakly dispersive magnon branches. We uncover fourfold and twofold degenerate modes which are almost flat on the $k_y k_z$ plane of reciprocal space, independent of the presence of 3D interchain exchange interactions. Furthermore, we demonstrate that 3D

magnetic order can develop from a fluctuating valence bond state as a consequence of specific relations between exchange interactions.

II. EXPERIMENTAL DETAILS

Raman scattering experiments were performed with different setups in quasibackscattering geometry on the as-grown surfaces of $Fe_2O(SeO_3)_2$ single crystals. We used an excitation wavelength $\lambda = 532.1$ nm of a Nd:YAG solid-state laser with the power $P = 2$ mW. The scattered light was collected and dispersed by a triple monochromator DILOR XY spectrometer onto a liquid-nitrogen-cooled Horiba Jobin Yvon, Spectrum One CCD-3000V detector. The temperature dependence of the Raman spectra was obtained in a variable temperature closed-cycle cryostat (Oxford/Cryomech Optistat). A Horiba LabRam HR800 spectrometer was used for measurements from the top of the needlelike sample with a regular size of $0.1 \times 0.1 \times 1$ mm^3. Raman spectra were measured in *aa*, *bb*, *cc*, *ac*, and *bc* scattering geometries.

III. EXPERIMENTAL RESULTS

$Fe_2O(SeO_3)_2$ crystallizes in the orthorhombic structure [28,29] (space group *Pccn*, No. 56, $Z = 8$) with the unit cell constants $a = 6.571(4)$ Å, $b = 12.83(1)$ Å, and $c = 13.28(1)$ Å. The structure consists of triangle-based magnetic
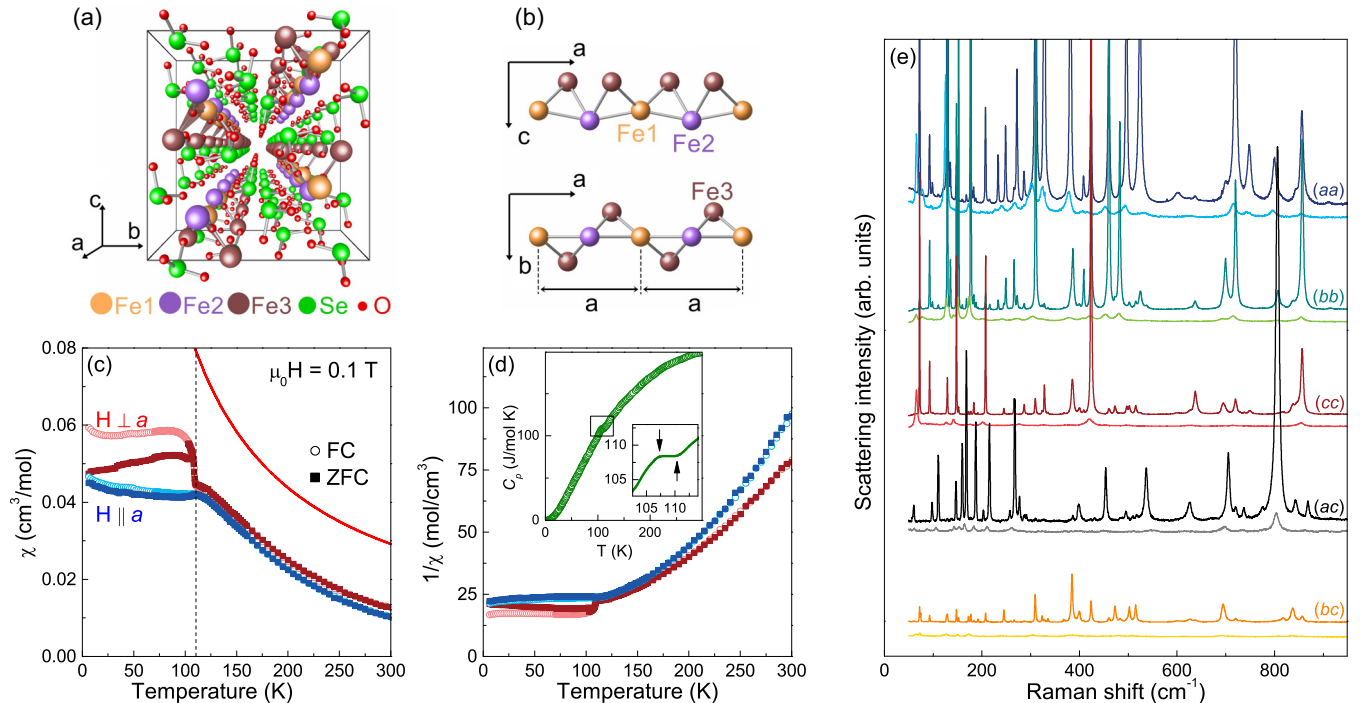

FIG. 1. (a) Crystal structure of $Fe_2O(SeO_3)_2$. Four saw-tooth chains in the primitive cell running along the *a* axis. (b) Saw-tooth arrangement of the Fe^{3+} ions. Basic triangular clusters are formed by three Fe^{3+} ions. Projections onto the *ab* plane and the *ac* plane of one representative saw-tooth chain are shown. The primitive unit cell contains 16 iron ions, which include one Fe1, one Fe2, and two Fe3 ions for each of the four chains. (c) Temperature dependence of the magnetic susceptibility χ obtained in field-cooled (open circles) and zero-field-cooled (solid squares) modes. The red line represents the Curie-Weiss law for noninteracting Fe^{3+} ions ($S = 5/2$, $\mu = 5.92\ \mu_B$). (d) Inverse magnetic susceptibility. The inset shows the temperature dependence of the specific heat capacity. (e) Raman spectra of $Fe_2O(SeO_3)_2$ taken at 290 and 6 K in five different scattering configurations.
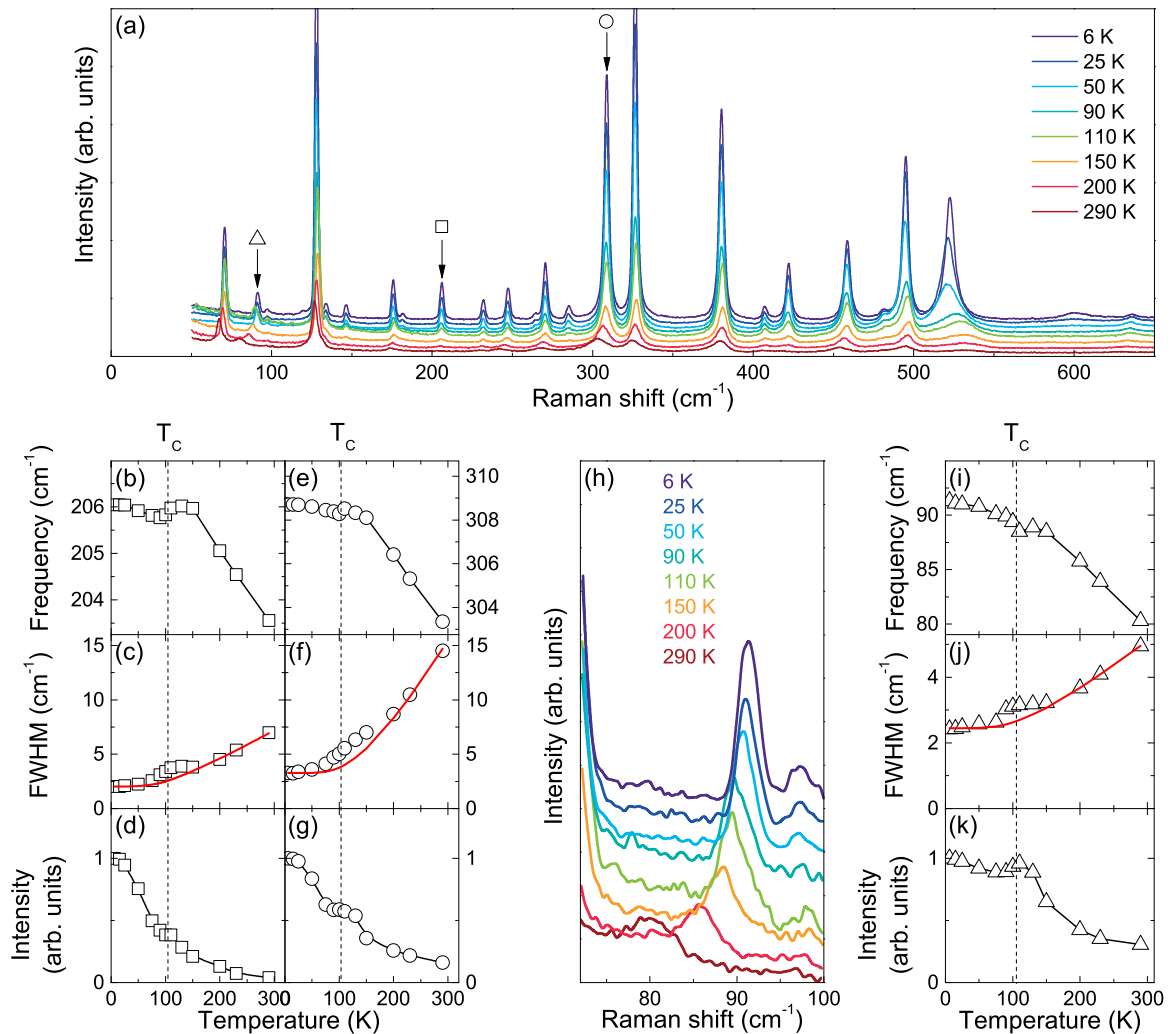
FIG. 2. (a) Temperature dependent Raman spectra of $Fe_2O(SeO_3)_2$ taken in aa scattering geometry. The open square, circle, and triangle mark the phonons detailed below. (b)–(g) Temperature dependence of selected phonon line parameters (frequency, width, and integrated intensity). The solid red lines represent temperature-induced anharmonic phonon behavior [30–32]. (h) Temperature dependence of the line at 80 cm^{-1} (at 290 K); (i)–(k) its extracted parameters (frequency, width, and integrated intensity).

chains made of $S = 5/2$ Fe^{3+} ions occupying three crystal-lographically distinct sites (Fe1, Fe2, and Fe3). Every tooth of these chains is centered by one oxygen atom, coordinating two octahedra $Fe1O_6$ and $Fe3O_6$, and one tetrahedron $Fe2O_4$. The Fe3 clusters that are connected to each other via Fe1 and Fe2 corners form the chains along the a axis with teeth alternatively tilted along different diagonals in the bc plane as shown in Fig. 1(b). The triangular Fe clusters sharing Fe1 and Fe2 corners form the saw-tooth-like chains, with their teeth alternatively tilted from the ac plane.

The temperature dependence of the magnetic suscepti-bility $\chi(T)$ of $Fe_2O(SeO_3)_2$ taken at $B = 0.1$ T is shown in Fig. 1(c). At high temperatures, field-cooled (FC) and zero-field-cooled (ZFC) curves coincide. The susceptibility increases with lowering temperature, culminating in a broad hump at approximately $T = 120$ K revealing the formation of short-range correlations that are not described by a Curie-Weiss law [see the $1/\chi(T)$ curves in Fig. 1(d)]. Below T_C,

the compound undergoes a magnetic phase transition into a long-range-ordered state. The low-temperature magnetic sus-ceptibility is finite, indicating antiferromagnetism. The total, as-measured specific heat, shown in the inset of Fig. 1(d), shows a rounded peak at T_C, confirming a magnetic phase transition. The ZFC curve measured with the magnetic field perpendicular to the a axis shows a sharp peak just below T_C. This may be related to a spin-flop transition in relatively low magnetic fields. A rapid increase of $\chi(T)$ below $T = 110$ K may indicate an additional ferromagnetic moment arising.

For an analysis of the coupling between lattice and spin degrees of freedom a complete knowledge of the vibra-tional properties of the material is essential. For the $Pccn$ orthorhombic structure of $Fe_2O(SeO_3)_2$ with three Fe ions located at the $4c$, $4d$, and $8e$ Wyckoff positions, and all selenium and oxygen ions at the $8e$ position [28], the factor group analysis gives a total of 132 Raman-active phonon modes: $\Gamma_{Raman} = 32A_g + 32B_{g} + 34B_{2g} + 34B_{3g}$. The Raman
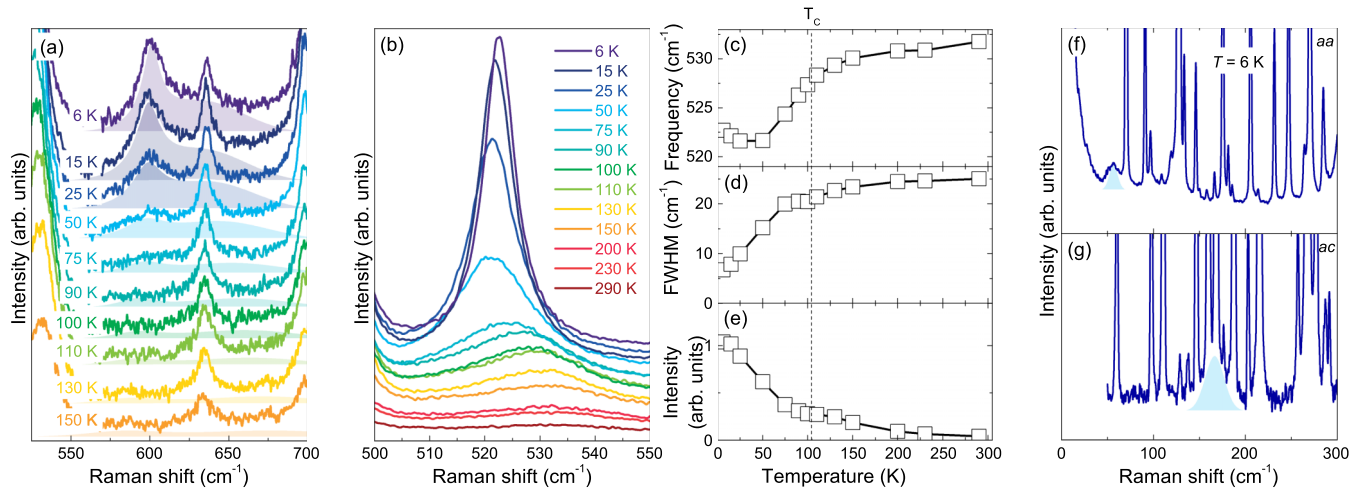
FIG. 3. (a) Two-magnon Raman signal obtained in *aa* polarization at various temperatures. Shaded areas mark the background of magnetic excitations. (b) Temperature dependence of the line at 523 cm^{-1}; (c)–(e) its parameters (frequency, width, and integrated intensity). (f) Low frequency magnetic excitations in the *aa* and (g) *ac* Raman spectra taken at $T = 6$ K.

tensors take the form

$$
A_g = \begin{pmatrix} a & 0 & 0 \\ 0 & b & 0 \\ 0 & 0 & c \end{pmatrix}, \quad B_g = \begin{pmatrix} 0 & d & 0 \\ d & 0 & 0 \\ 0 & 0 & 0 \end{pmatrix},
$$

$$
B_{2g} = \begin{pmatrix} 0 & 0 & e \\ 0 & 0 & 0 \\ e & 0 & 0 \end{pmatrix}, \quad B_{3g} = \begin{pmatrix} 0 & 0 & 0 \\ 0 & 0 & f \\ 0 & f & 0 \end{pmatrix}. \quad (1)
$$

We find that the Raman spectra of $Fe_2O(SeO_3)_2$ at $T = 290$ and 6 K are very well polarized [see Fig. 1(e)]. Narrow and well-distinguishable phonon peaks (accounting for a high sample quality) with various intensities are observed. In the frequency range of 10–900 cm^{-1} and at $T = 6$ K all 100 Γ-point Raman-active phonon modes of A_g, B_{2g}, and B_{3g} symmetry can be clearly identified. In addition, very weak

and broad second order excitations are observed in the higher frequency regime up to 1300 cm^{-1} (not shown).

The temperature dependence of the Raman spectra of $Fe_2O(SeO_3)_2$ obtained in *aa* scattering geometry is shown in Fig. 2(a) and an in-depth analysis providing several distinct features is given in Figs. 2(b)–2(g). First, the phonon eigen-frequencies trace the temperature dependence of the magnetic subsystem, showing a broad hump at approximately 120 K and a jump in frequency at T_C. This renormalization of the phonon frequency and linewidth should be ascribed to a direct contribution of an exchange coupling to the quasielastic constant of the mode, i.e., spin-phonon coupling. The deviation of the phonon linewidth behavior from an expected anharmonic broadening in the temperature region of 75–150 K suggests a change of the relaxation mechanism. Furthermore, the most remarkable feature is the pronounced enhancement of phonon intensities, which grow by almost one order of magnitude

TABLE I. Magnetic excitations in $Fe_2O(SeO_3)_2$.

| Frequency ($T = 6$ K, cm^{-1})	Width ($T = 6$ K, HWHM, cm^{-1})	Pol.	Properties	Tentative assignment
54.7	12	*aa*	Chain specific pol.	Two formerly flat-band zero energy magnons
166.6	25	*ac*	Crossed pol.	High energy + one of the activated zero energy flat-band magnons
522.7	7	*aa*	Visible up to $T = 295$ K, linewidth twice as large as the phonon lines, chain specific pol.	High energy + one of the activated zero energy flat-band magnons
620	< 100	*aa*	Two components, 601 and 634.5 cm^{-1}, broad maximum, visible up to 150 K, anomalous frequency, width, and intensity, chain specific pol.	High energy + one of the activated zero energy flat-band magnons
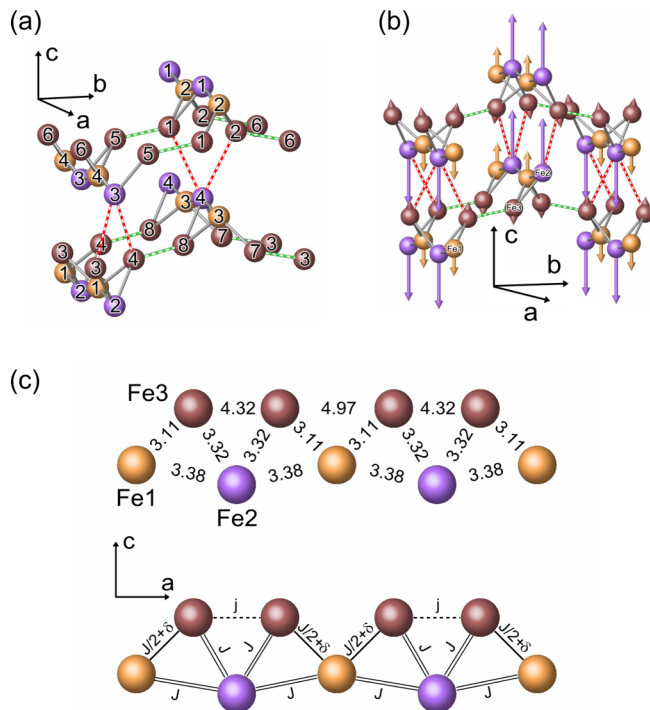
FIG. 4. (a) Schematics of the magnetic Fe^{3+} ion positions in $Fe_2O(SeO_3)_2$. All oxygen and selenium ions are omitted for clarity. The Fe ions in $4c$, $4d$, and $8e$ Wyckoff sites are shown in gold, violet, and dark brown, respectively. The intralayer interchain exchanges are marked by dashed green lines. The interlayer interactions are realized through Fe2-O-Se-O-Fe3 bonds and highlighted by dashed red lines. The accepted enumeration of Fe ions is shown. (b) Vibrational pattern of the low-frequency A_g mode experimentally observed at frequencies of 80–92 cm^{-1}. For clarity only Fe^{3+} ions are shown. The length of arrows represents relative amplitudes of out-of-phase motion of the Fe2 and Fe3 ions from the neighboring Fe^{3+} layers. (c) Mapping of the structure on a saw-tooth magnetic unit. The oxygen and selenium ions are omitted for clarity. A possible approximation of exchange constants is shown. Note that the saw-tooth chain includes two different teeth instead of a single tooth in the usual saw-tooth chain. This double-tooth chain requests four magnetic ions for a minimal model.

upon cooling from room temperature to 6 K with a deviation from their smooth behavior in the same temperature region where linewidth anomalies appear. Similarly, an anomalous increase in the intensity of the phonon lines upon cooling was observed earlier in multiferroic compounds Cu_2OSeO_3 [33] and $FeTe_2O_5Br$ [34] and was unambiguously attributed to an increase of the respective electronic polarizability with temperature. Our observations indicate strong spin-lattice coupling in $Fe_2O(SeO_3)_2$.

An exception is the behavior of the low-frequency phonon mode at 80 cm^{-1} (295 K). It hardens by more than 10 cm^{-1} upon cooling from 290 to 6 K [see Figs. 2(h)–2(i)], which is several times larger than the hardening of the remaining phonon lines. This indicates that this excitation responds especially strong to magnetic ordering.

The most striking observation in our experiment is the set of bands appearing at low temperatures and observable

only in aa polarization at 54, 523, and 600 cm^{-1}, and a further excitation at 163 cm^{-1} in ac polarization. Their unique temperature dependence allows us to assign them to two-magnon Raman scattering processes related to 3D long-range order in $Fe_2O(SeO_3)_2$ (see Fig. 3).

The broad two-humped feature with a strong maximum centered at around 600 cm^{-1} in the spectrum at 6 K demonstrates a typical two-magnon behavior: It softens in frequency and broadens in linewidth upon increasing temperature and strongly drops in intensity for $T > T_C$, although it remains distinguishable up to 150 K [see Fig. 3(a)]. Accordingly, short-range spin correlations within the chain survive up to $T = 1.4T_C$.

The excitation at 523 cm^{-1} [Fig. 3(b)] has a comparably smaller linewidth and remains distinguishable even at room temperature. With lowering temperature its linewidth decreases in an unusual way [see Fig. 3(d)] with a local minimum at T_C. With further cooling, the line begins to harden below approximately 35 K [Fig. 3(c)]. Its line shape changes with decreasing temperature from asymmetric to symmetric. Tentatively we may assign this well-defined peak to a magnetic excitation, i.e., due to singularities of the one-dimensional density of two-magnon states [35]. The unusual narrow linewidth of this signal can be connected with a specific flatness of the magnetic spectrum in $Fe_2O(SeO_3)_2$. The observation of this excitation in aa polarization (i.e., along the saw-tooth chain direction) is typical for spin-chain compounds and supports our tentative assignment [36]. Similar excitations related to the magnetic dimer structure were observed, e.g., in MgV_2O_5 [35] and $BaFe_2Se_2O$ [37].

Another relatively narrow magnetic signal appears below T_C at 54 cm^{-1}, which is one order of magnitude smaller than the energy scale of the previous magnetic signals [see Fig. 3(f)]. The signal is highly polarized and is seen only in aa polarization. In addition, a signal seen at 163 cm^{-1} in crossed polarization [see Fig. 3(g)] also has a relatively narrow linewidth. Its observation in crossed ac polarization reflects the specific structure of the saw-tooth units with comparable distances between magnetic ions along a and c directions. In crossed polarization magnetic excitations of different symmetry can contribute to the Raman signal [29,38,39]. Therefore, its position represents some new energy scale existing in the magnetic spectrum of $Fe_2O(SeO_3)_2$. We summarize all magnetic modes and their properties in Table I.

The observed signals share some general feature—their relatively narrow linewidth compared to the scale of exchange that follows from the rather high T_C. Since there are 16 magnetic Fe ions per unit cell, the spin-wave spectrum of $Fe_2O(SeO_3)_2$ contains 16 branches [see Figs. 1(a) and 1(b)]. The unusual diversity of two-magnon bands by energy evidences a strict separation of the spin-wave spectrum into low and high energy spin waves without any overlapping in between. The narrow linewidth of the two-magnon bands indicates the existence of flat regions in the magnetic spectrum. All of this is a hallmark of the saw-tooth lattice and a magnetic structure where low energy excitations originate from formerly zero energy flat-band modes. In the following we will discuss these features in detail.

IV. DISCUSSION

We will first focus on structural details of $Fe_2O(SeO_3)_2$ which affect the aforementioned properties. The Fe ions build up the four saw-tooth chains that are running along the *a* axis. The spin chain is formed by a sequence of corner-sharing $Fe1O_6$ octahedra and $Fe2O_4$ tetrahedra. The tilted teeth of the chain are formed by $Fe3O_6$ oxygen octahedra which are connected to $Fe1O_6$ octahedra by edge sharing. The saw-tooth chains connect to each other along the *b* axis by edge-sharing $Fe3O_6$ octahedra. Along the *c* axis the saw-tooth chains are connected via $(SeO_3)^{2-}$ complexes changing the Fe-O-Fe exchange pathway into a longer Fe-O-Se-O-Fe one, as sketched in Fig. 4(a).

Looking at the arrangement of magnetic bonds (e.g., in the approximation of nearest-neighbor exchange interactions) one can sort out two weakly coupled Fe^{3+} *ab* planes which are formed by two saw-tooth chains running along the *a* axis. The interaction between these chains is weaker than the intrachain interactions. Indeed, the angle of the Fe1-O-Fe2 bonds in corner-shared octahedra along the spine of chains is larger than the angle of the Fe3-O-Fe3 bonds in edge-shared octahedra connecting neighboring saw-tooth chains. In contrast, the corner-shared Fe2-O-Fe3 intrachain interaction between vertex and spine Fe ions remains comparable with Fe1-O-Fe2 interactions. This hierarchy supposes that the one-dimensional (1D) saw-tooth chain is the main magnetic unit in $Fe_2O(SeO_3)_2$, and the interplane Fe2-O-Se-O-Fe3 exchange interaction should be responsible for the 3D long-range ordering.

Our Raman data [see Figs. 2(h)–2(k)] and lattice dynamic calculations [see Fig. 4(b)] strongly support the assumption that the phonon mode corresponding to out-of-phase motions of the Fe2 and two Fe3 ions from neighboring Fe^{3+} *ab* planes should be highly sensitive to 3D magnetic order. As we have shown by our lattice dynamical calculations, one of the lowest-frequency Raman modes of A_g symmetry (at 80 cm^{-1}) represents the displacements of Fe2 ions along the *z* axis. In neighboring (along *y* direction) chains these displacements are antiphase [29,40]. In such a type of motion, the distance varies along the *z* direction between neighboring Fe2 and Fe3 ions. Their exchange coupling provides the three-dimensional magnetic ordering and leads to a renormalization of this phonon mode.

The susceptibility measurements suggest that below T_C the magnetic long-range order is antiferromagnetic [see Figs. 1(c) and 1(d)], and the easy axis (i.e., main antiferromagnetic vector) should be perpendicular to the *a* axis. Measurements perpendicular to the *a* axis show that the applied magnetic field has components both perpendicular and parallel to this easy axis. An anomalous increase of the susceptibility just below T_C as well as the large difference for FC and ZFC data can be interpreted as a presence of a weak ferromagnetic moment which points perpendicular to the *a* axis. However, the development of an incommensurate magnetic structure can also be a cause of the susceptibility anomalies. An increase of electronic polarizability below T_C, which is detected in our Raman spectra, points to such a possibility. Only an incommensurate magnetic order can be a source of electronic polarization in the crystal with space inversion symmetry [41].

Figure 4(c) illustrates the saw-tooth chain unit including the distances between Fe ions. The mutual relations of exchange interaction constants can be roughly estimated based on the type and angles of the Fe-O-Fe bonding. Note that Fe1-Fe2 and Fe2-Fe3 ions are connected through corner-shared octahedra while Fe1-Fe3 ions are connected through edge-shared octahedra. The Fe3-Fe3 exchange is realized through a Fe-O-Se-O-Fe pathway.

Here we assume that Fe1-Fe2 (with an angle of Fe1-O-Fe2 = 127.79°) and Fe2-Fe3 (with an angle of Fe2-O-Fe3 = 123.7°) are bonded by the same AFM exchange. The Fe1-Fe3 bonding is weaker, as it forms through Fe1-O2-Fe3 plaquettes of edge-shared Fe1 and Fe3 octahedra with both angles Fe-O-Fe (Fe-O'-Fe = 93.24° and Fe-O''-Fe = 107.95°) being closer to the critical value where the exchange interaction changes
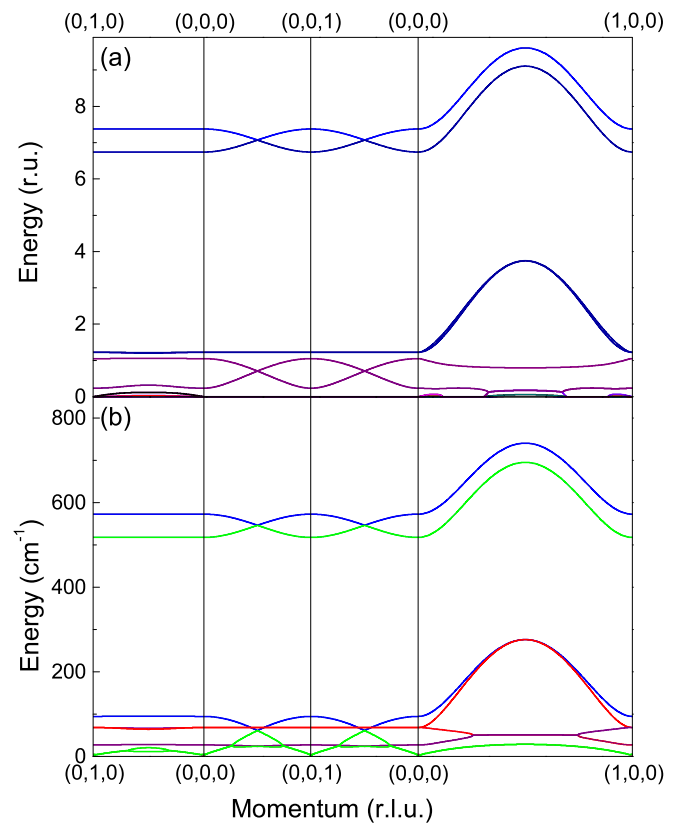

FIG. 5. (a) One-magnon spectrum along high symmetry lines of four coupled saw-tooth chains mapped to the minimal model in Fig. 4(c). The Fe1-Fe2 exchange J is selected as the energy unit, and the AFM intralayer exchange $I_l = 0.1J$, the interlayer AFM exchange $I_p = 0.1J$, the vertex-vertex (Fe3-Fe3) AFM exchange $j = 0.1J$, and $\delta = 0$. The development of the incommensurable instability along the *a* axis is seen as the appearance of zero frequencies at a certain wave vector along (100). This wave vector will be the helix wave vector. (b) The calculated one-magnon spectrum for exchange parameters estimated from two-magnon signals. The blue and green colors denote double degenerate magnon branches which have the same symmetry at $k = 0$. The double degenerate Goldstone modes (in green color) merge with the two lowest gapped branches with the gap at 5 cm^{-1}. The red color denote the four degenerate and almost flat-band modes along the (010) and (001) directions. Similar double-degenerate flat-band mode is seen at 27 cm^{-1}.

sign. The Fe3-O-Se-O-Fe3 exchange j between the tooth's vertices with a distance of 4.32 Å is supposed to be nonzero as it has the same origin as the interlayer Fe2-O-Se-O-Fe3 exchange with a distance of 4.64 Å. It is worth repeating that this last interaction is responsible for establishing long-range order.

To elucidate the general structure of the magnon spectrum and to check the stability of uniform magnetic order we proceed with the one-magnon spectra calculation with small variations of the δ and j constants compared to the exchange J and supposing that the interlayer exchange I_p and intralayer exchange I_l can be either FM or AFM. A detailed analysis of possible types of uniform exchange magnetic long-range order in $Fe_2O(SeO_3)_2$ is presented in the Supplemental Material [29]. The calculations have been performed in linear spin wave (LSW) approximation with the help of the SpinW code [42]. The LSW theory can capture an incommensurate instability of the given 3D uniform long-range order under detection of some spin wave approaching zero energy at a certain wave vector. An example of a spin wave spectrum with an incommensurate instability of the initial collinear phase with both I_p and I_l being AFM (Γ_4 phase) is shown in Fig. 5(a).

The respective numerical analysis has been done for all four uniform structures which can be realized for different signs of interlayer (I_p) and intralayer (I_l) interchain exchanges [29]. We conclude that the structure with an AFM intralayer exchange $I_l > 0$ and AFM interlayer exchange $I_p > 0$ supports the development of an incommensurate magnetic order. A uniform exchange structure with ferromagnetic interlayer exchange $I_p < 0$ and $I_l > 0$ (Γ_2 phase) can be stable if the modulus of $|I_p|$ is above a certain threshold which is roughly one order smaller than the Fe1-Fe3 intrachain interaction. The uniform exchange magnetic structures with the ferromagnetic intralayer interchain exchange $I_l < 0$ are always stable, irrespective of the sign of the interlayer exchange (Γ_1 phase and Γ_3 phase). Thus, in the following we will consider as a starting point the Γ_4 phase, with all exchanges positive, as a classical ground state of the system.

The above mapping shows a distinct difference in the topology of the exchange patterns of the saw-tooth chain in $Fe_2O(SeO_3)_2$ compared to a standard saw-tooth chain (Δ chain) with equal values of the exchange interactions between spine and vertex (e.g., for the case $\delta = J/2$ and $j = 0$) [1–3]. One may check the existence of zero-energy flat-band modes in the classical limit for the isolated, noninteracting saw-tooth unit in $Fe_2O(SeO_3)_2$ [see Fig. 4(c)]. Most unusual is the presence of double degenerate zero-energy flat-band modes in the case of $j = 0$ and $\delta = 0$. This feature is related to four magnetic ions in the primitive cell of the saw-tooth unit instead of two ions in the Δ chain. In the case of $j \neq 0$ and $\delta = 0$ one flat-band mode survives and one Goldstone mode appears. Two high energy modes emerge with energies of $2.5SJ$ and $S(J/2 - 2j)$ at the Γ point. No flat-band modes exist for $\delta \neq 0$ independently of the value of j. Note that the presence of the vertex-vertex interaction j does not contribute to a gap formation. Furthermore, the zero-energy flat-band modes disappear in the case of different values of J_{bb} (spine-spine, Fe1-Fe2) and J_{bv} (spine-vertexes, Fe2-Fe3) exchange.

The activated flat-band modes remain weakly dispersive with a gap dependent on δ and the difference $J_{bb} - J_{bv}$.

In the classical limit the spin wave spectrum of interacting saw-tooth units in $Fe_2O(SeO_3)_2$ with I_l, $I_p \ll J$ is separated into several energy regions. It is dominated by the presence of a few high-energy SW branches and a large number of low-energy SW branches, which partially originate from formerly zero-energy flat-band modes. In contrast to conventional 3D antiferromagnets the spin waves from different energy regions do not overlap in k space.

The flat-band modes survive for the two-dimensional (2D) and 3D structures of interacting saw-tooth chains with $\delta = 0$. Note that for noninteracting four saw-tooth units in the crystallographic unit cell of $Fe_2O(SeO_3)_2$ every mode will be fourfold degenerate. In the 2D ab layer of saw-tooth chains interacting through the interchain exchange I_l the zero-energy flat mode survives along the (010) direction. In the 2D ac layer of saw-tooth chains connected through I_p exchange along the (001) direction, the double-degenerate zero-energy flat-band mode exists in the (001) direction. These modes survive along the (001) direction even in the 3D case with both nonzero I_p and I_l exchanges, whereas zero-energy flat-band modes along the (010) direction are absent. The respective model spectrum is shown in Fig. 5(a).

The value of δ defines the activation energy of the formerly zero-energy flat-band modes. We find the fourfold degenerate SW at an energy of $S\sqrt{E(E + 2I_l)}$ at $k = 0$, where $E = J/2 - 2j - \delta + I_p$ remains almost nondispersive along the (010) and (001) directions under arbitrary values of 3D interchain couplings. The energetically highest fourfold degenerate modes split into two double degenerate modes under consideration of interlayer interchain coupling I_p. We reveal that the splitting linearly depends on the value I_p. The dispersion of high-energy modes in the Heisenberg approximation does not show any obvious sensitivity to the underlying incommensurate order.

The observed two-magnon Raman bands contain an unusual combination of high- and low-energy magnon branches. The necessary symmetry conditions for two-magnon scattering in parallel aa polarization are fulfilled to obey such a contribution. Indeed, every four (out of 16) magnon branches have the same symmetry along (100), (010), and (001) directions in the Brillouin zone, and every set of branches with the same symmetry includes at least one high-energy branch and at least two low-energy branches. The specific saw-tooth structure allows two-magnon scattering in the nondiagonal ac polarization with the participation of two-magnon branches of different symmetry. The quasi-1D exchange topology in $Fe_2O(SeO_3)_2$ implies a very weak magnon dispersion perpendicular to the spine of chains that forms a high density of states for spin waves with energies close to the Γ point. We conclude that the energy scale of the two-magnon bands in $Fe_2O(SeO_3)_2$ observed in our Raman data is given by magnon energies at the Γ point and not at the Brillouin zone boundaries as is realized in conventional 3D antiferromagnets. The anomalous narrow linewidth of the two-magnon bands, comparable with the phonon linewidth, can be explained by the flatness of spin waves contributing to the scattering process.

Energies of the spin waves at the Γ point have been calculated analytically in the nearest neighbor Heisenberg approximation [29]. Using this approach, we estimate the exchange constants of $Fe_2O(SeO_3)_2$: $J = 75.84$ cm^{-1}; $I_p = 9.18$ cm^{-1}; $j = 12.1$ cm^{-1}; $I_l = 10$ cm^{-1} and $\delta = 3.77$ cm^{-1}. Based on these exchange energies we estimate the Néel temperature $T_N = 103$–106 K, i.e., fully coinciding with the experiment. The restored spin wave spectrum of $Fe_2O(SeO_3)_2$ is shown in Fig. 5(b). The spectrum does not show any incommensurate instability for the given choice of parameters. However, a small variation of the interlayer interchain exchange I_p and a respective change of the ratio j/I_p both introduce incommensurability along the (100) direction. There are two flat-band modes almost dispersionless on $k_y k_z$ plane of k space at 68.4 and 27 cm^{-1} present in the spectrum. A very weak dispersion for these modes is observed along the (010) direction.

These interaction constants with antiferromagnetic vertex-vertex interaction highlight the strong degree of frustration existing in $Fe_2O(SeO_3)_2$. At the same time they may provide an explanation of the instability of the fluctuating quantum dimer state. Indeed, a simple analysis of the experimental magnetic susceptibility shows that in the range between T_C and 300 K the magnitude of $\chi_{expt}(T)$ lies far below $\chi_{CW}(T)$ [see Fig. 1(c)], which accounts for the Curie-Weiss susceptibility of 16 unbound Fe^{3+} ions (eight formula units per primitive cell). This discrepancy can be unambiguously attributed to the presence of various dynamic valence bonds in their singlet ground states and with a high enough energy of its excited magnetic levels. Therefore, they do not contribute to the magnetic susceptibility. However, in spite of the relatively low values of the interchain interactions which validate the 1D approximation, we found that the ratio of spine-vertex (Fe1-Fe3) to spine-spine (Fe1-Fe2) interactions $J_{bv}/J_{bb} = (J/2 + \delta)/J$ is close to 1/2. As pointed out in Ref. [4], the difference in J_{bb} and J_{bv} interactions leads to a suppression of the spin gap in the quantum limit for the $S = 1/2$ saw-tooth model chain with a dimer ground state. The spin gap approaches zero at $k = 0$ for J_{bb}/J_{bv} close to 0.5 and at $k = \pi$ for J_{bb}/J_{bv} close to 1.5. The previously dispersionless $S = 1$ excitations become highly dispersive and the system turns into Heisenberg chains.

Taking DM interaction into account should have a similar influence, even if $J_{bb} = J_{bv}$. As shown in Ref. [7], a relatively weak DMI of $\sim 0.1 J_{bb}$ is sufficient to destroy the valence-bond order, to close the spin gap, and to turn the system into a Luttinger liquid with incommensurate spin correlations and spin-wave excitations. In $Fe_2O(SeO_3)_2$ DMI contributes to all Fe-Fe magnetic bonds. As follows from bond symmetry the DM vector for the Fe1-F2 spine-spine magnetic bonds is directed purely along the z axis, whereas for all other bonds it has all Cartesian components. To this point one can add that DMI also supports the onset of an incommensurable instability of a uniform 3D long-range order. In the classical limit, the presence of DM interaction forms a spiral order in the usual $S = 1/2$ saw-tooth chain [7]. Note that DMIs were not included in the above considerations as we show by model calculations that the incommensurate instability in $Fe_2O(SeO_3)_2$ can be induced already in the Heisenberg exchange approximation.

V. SUMMARY

In the saw-tooth spin-chain system $Fe_2O(SeO_3)_2$ long-range magnetic order is established below $T_C = 105$ K, as confirmed by anomalies in specific heat and magnetic susceptibility. Raman-active A_g phonon modes show anomalies in linewidths and energies close to T_C. The A_g mode at 80 cm^{-1}, which constitutes the out-of-phase motion of the Fe ions from neighboring Fe layers, is especially sensitive to the onset of 3D order. An anomalous increase of phonon intensities below T_C points towards an increase of the electronic polarizability. We conclude an incommensurability of the magnetic 3D order in $Fe_2O(SeO_3)_2$ which would give rise to electronic polarization in a crystal with space inversion symmetry.

Excitations related to long-range magnetic order exist with polarization along the chain direction with a pronounced temperature dependence. We assign them to two-magnon signals. These excitations are strongly differentiated in energy with relatively small linewidth in contrast to a widely spread continuum which is expected from the high T_C of this compound. We connect these features to the specific form of the one-magnon spectrum of the saw-tooth magnetic lattice with a set of dispersionless spin-wave branches. The minimal set of exchange coupling constants has been roughly estimated based on Raman data and results of linear spin-wave calculations. The onset of the incommensurate 3D magnetic order and the vanishing of the dimer quantum state in the highly frustrated title compound may result from the specific relations between given exchange interactions. We show that in the classical limit the one-magnon spectrum of $Fe_2O(SeO_3)_2$ contains a few almost flat-band modes in the $k_y k_z$ plane of k space.

[1] K. Kubo, Phys. Rev. B **48**, 10552 (1993).

[2] T. Nakamura and K. Kubo, Phys. Rev. B **53**, 6393 (1996).

[3] D. Sen, B. S. Shastry, R. E. Walstedt, and R. J. Cava, Phys. Rev. B **53**, 6401 (1996).

[4] S. A. Blundell and M. D. Núñez-Regueiro, Eur. Phys. J. B **31**, 453 (2003).

[5] V. Ohanyan, Condens. Matter Phys. **12**, 343 (2009).

[6] S. Bellucci and V. Ohanyan, Eur. Phys. J. B **75**, 531 (2010).

[7] Z. Hao, Y. Wan, I. Rousochatzakis, J. Wildeboer, A. Seidel, F. Mila, and O. Tchernyshyov, Phys. Rev. B **84**, 094452 (2011).

[8] V. R. Chandra, D. Sen, N. B. Ivanov, and J. Richter, Phys. Rev. B **69**, 214406 (2004).

[9] M. E. Zhitomirsky and H. Tsunetsugu, Phys. Rev. B **70**, 100403(R) (2004).

[10] M. E. Zhitomirsky and H. Tsunetsugu, Prog. Theor. Phys. Suppl. **160**, 361 (2005).

[11] O. Derzhko, J. Richter, and M. Maksymenko, Int. J. Mod. Phys. B **29**, 1530007 (2015).

[12] E. J. Bergholtz and Z. Liu, Int. J. Mod. Phys. B **27**, 1330017 (2013).

[13] D. Leykam and S. Flach, APL Photon. **3**, 070901 (2018).

[14] R. A. Vicencio, C. Cantillano, L. Morales-Inostroza, B. Real, C. Mejía-Cortés, S. Weimann, A. Szameit, and M. I. Molina, Phys. Rev. Lett. **114**, 245503 (2015).

[15] X. S. Wang, H. W. Zhang, and X. R. Wang, Phys. Rev. Appl. **9**, 024029 (2018).

[16] S. Weimann, L. Morales-Inostroza, B. Real, C. Cantillano, A. Szameit, and R. A. Vicencio, Opt. Lett. **41**, 2414 (2016).

[17] R. Chisnell, J. S. Helton, D. E. Freedman, D. K. Singh, R. I. Bewley, D. G. Nocera, and Y. S. Lee, Phys. Rev. Lett. **115**, 147201 (2015).

[18] R. J. Cava, H. W. Zandbergen, A. P. Ramirez, H. Takagi, C. T. Chen, J. J. Krajewski, W. F. Peck, Jr., J. V. Waszczak, G. Meigs, R. S. Roth, and L. F. Schneemeyer, J. Solid State Chem. **104**, 437 (1993).

[19] O. Le Bacq, A. Pasturel, C. Lacroix, and M. D. Núñez-Regueiro, Phys. Rev. B **71**, 014432 (2005).

[20] G. C. Lau, B. G. Ueland, R. S. Freitas, M. L. Dahlberg, P. Schiffer, and R. J. Cava, Phys. Rev. B **73**, 012413 (2006).

[21] J. S. White, T. Honda, K. Kimura, T. Kimura, Ch. Niedermayer, O. Zaharko, A. Poole, B. Roessli, and M. Kenzelmann, Phys. Rev. Lett. **108**, 077204 (2012).

[22] T. Honda, Y. Ishiguro, H. Nakamura, Y. Wakabayashi, and T. Kimura, J. Phys. Soc. Jpn. **81**, 103703 (2012).

[23] T. Honda, J. S. White, A. B. Harris, L. C. Chapon, A. Fennell, B. Roessli, O. Zaharko, Y. Murakami, M. Kenzelmann, and T. Kimura, Nat. Commun. **8**, 15457 (2017).

[24] H. Kikuchi, Y. Fujii, D. Takahashi, M. Azuma, Y. Shimakawa, T. Taniguchi, A. Matsuo, and K. Kindo, J. Phys.: Conf. Ser. **320**, 012045 (2011).

[25] A. F. May, S. Calder, D. S. Parker, B. C. Sales, and M. A. McGuire, Sci. Rep. **6**, 35325 (2016).

[26] V. O. Garlea, L. D. Sanjeewa, M. A. McGuire, P. Kumar, D. Sulejmanovic, J. He, and S.-J. Hwu, Phys. Rev. B **89**, 014426 (2014).

[27] A. Baniodeh, N. Magnani, Y. Lan, G. Buth, C. E. Anson, J. Richter, M. Affronte, J. Schnack, and A. K. Powell, npj Quantum Mater. **3**, 10 (2018).

[28] G. Giester, Z. Kristallographie **211**, 603 (1996).

[29] See Supplemental Material at http://link.aps.org/supplemental/10.1103/PhysRevB.99.064413 for details on crystal growth, lattice dynamical calculations, and symmetry analysis.

[30] K. Wakamura and T. Arai, J. Appl. Phys. **63**, 5824 (1988).

[31] P. G. Klemens, Phys. Rev. **148**, 845 (1966).

[32] M. Balkanski, R. F. Wallis, and E. Haro, Phys. Rev. B **28**, 1928 (1983).

[33] V. P. Gnezdilov, K. V. Lamonova, Yu. G. Pashkevich, P. Lemmens, H. Berger, F. Bussy, and S. L. Gnatchenko, Low Temp. Phys. **36**, 550 (2010).

[34] K.-Y. Choi, I. H. Choi, P. Lemmens, J. van Tol, and H. Berger, J. Phys.: Condens. Matter **26**, 086001 (2014).

[35] M. J. Konstantinović, Z. V. Popović, M. Isobe, and Y. Ueda, Phys. Rev. B **61**, 15185 (2000).

[36] P. Lemmens, G. Günterodt, and C. Gros, Phys. Rep. **375**, 1 (2003).

[37] Z. V. Popović, M. Šćepanović, N. Lazarević, M. M. Radonjić, D. Tanasković, H. Lei, and C. Petrovic, Phys. Rev. B **89**, 014301 (2014).

[38] A. Fleury and R. Loudon, Phys. Rev. **166**, 514 (1968).

[39] O. Cepas, J. O. Haerter, and C. Lhuillier, Phys. Rev. B **77**, 172406 (2008).

[40] G. D. Gale, Faraday Trans. **93**, 629 (1997).

[41] For a review see, e.g., A. B. Harris, J. Appl. Phys. **99**, 08E303 (2006).

[42] S. Toth and B. Lake, J. Phys. Condens. Matter **27**, 166002 (2015).